Atmos. Chem. Phys., 25, 16387–16399, 2025 https://doi.org/10.5194/acp-25-16387-2025 © Author(s) 2025. This work is distributed under the Creative Commons Attribution 4.0 License.





Underestimation of atmospheric oxidized mercury at a mountaintop site by the GEOS-Chem chemical transport model

Tyler R. Elgiar^{1,a}, Loknath Dhar^{1,2}, Lynne Gratz³, A. Gannet Hallar⁴, Rainer Volkamer⁵, and Seth N. Lyman^{1,2}

¹Bingham Research Center, Utah State University, Vernal, Utah 84078, USA
²Department of Chemistry and Biochemistry, Utah State University, Logan, Utah 84322, USA
³Chemistry Department & Environmental Studies Program, Reed College, Portland, Oregon 97202, USA
⁴Department of Atmospheric Sciences, University of Utah, Salt Lake City, Utah 84112, USA
⁵Department of Chemistry & CIRES, University of Colorado Boulder, Boulder, Colorado 80309, USA
^anow at: U.S. Bureau of Land Management, Vernal, Utah 84078, USA

Correspondence: Seth N. Lyman (seth.lyman@usu.edu)

Received: 28 February 2025 – Discussion started: 21 March 2025 Revised: 25 September 2025 – Accepted: 21 October 2025 – Published: 21 November 2025

Abstract. An improved mechanistic model of mercury redox chemistry has recently been implemented in the GEOS-Chem model. In this study, GEOS-Chem simulations were compared to ambient measurements made during a high-oxidized mercury episode that originated in the free troposphere at a mountaintop site in Colorado, USA $(40.455^{\circ} \text{ N}, -106.744^{\circ} \text{ W}, 3220 \text{ m}$ above sea level). Measurements were collected with a dual channel atmospheric oxidized mercury measurement system that has been shown to accurately quantify oxidized mercury compounds in ambient air. The model and observations showed similar temporal trends for elemental and oxidized mercury $(R^2 \text{ of } 0.54 \text{ to } 0.79)$ and similar elemental mercury concentrations (normalized mean square error of 0.04 in the base model). However, the base model only produced 17% of the maximum oxidized mercury observed in the dual channel system. In sensitivity tests with increased oxidation rates, the model still only produced, at most, 23% of maximum observed oxidized mercury. In addition to underestimating net mercury oxidation, an analysis of elemental to oxidized mercury slopes indicated the model overestimated oxidized mercury deposition. An analysis of GEOS-Chem results from a separate study confirmed that while GEOS-Chem is able to simulate the range of measured oxidized mercury in low-oxidized mercury episodes and locations it consistently underestimates measured values during high-oxidized mercury periods at surface locations in western USA.

1 Introduction

Mercury (Hg) is a globally distributed toxicant that has the potential to harm ecosystem, wildlife, and human health (Mahbub et al., 2017; Rice et al., 2014). Mercury is found ubiquitously throughout the environment and exists in the atmosphere as elemental Hg (Hg⁰) and oxidized Hg (denoted as Hg^{II} because almost all is believed to be in the +2-oxidation state; Shah et al., 2021). Mercury is emitted into the atmosphere by natural (e.g., volcanic activ-

ity and biomass burning) and anthropogenic (e.g., coal fire power plants and artisanal gold mining) sources as either Hg⁰ or Hg^{II} and can dynamically convert between the two forms (Jiao and Dibble, 2017a; Lam et al., 2019; Streets et al., 2019). Hg⁰ is relatively inert, but it can deposit to soil and plant surfaces (Zhou and Obrist, 2021). Hg^{II} is soluble and only sparingly volatile, allowing it to be readily deposited to any surface (Lyman et al., 2020a).

Most previous measurements of atmospheric Hg^{II} were made with commercial systems that utilize a KCl-coated de-

nuder; however, these are known to suffer from a low bias, the extent of which depends on atmospheric conditions (Lyman et al., 2010; McClure et al., 2014; Bu et al., 2018; Tang et al., 2022; Huang and Gustin, 2015). Cation exchange membrane-based systems have since been shown to avoid the low bias created by the KCl-coated denuder and have been deployed in locations around the globe (Tang et al., 2022; Luippold et al., 2020; Derry et al., 2024; Lyman et al., 2022; Gratz et al., 2015; Dunham-Cheatham et al., 2023). Although measurements of HgII are improving, current instrumentation is not compound specific; thus, many uncertainties surround the redox chemistry of atmospheric Hg (Jiao and Dibble, 2017b; Peng et al., 2021; Saiz-Lopez et al., 2019, 2020). Bromine (Br) and hydroxyl (OH) radicals are currently assumed to be the only primary oxidants of Hg⁰ that are significant in the ambient atmosphere (Fu et al., 2024; Castro et al., 2022). Oxidation of Hg^0 is understood to occur via a two-step process by which Hg^0 is first oxidized by Br or OH to form HgI radicals and then further oxidized by O₃ and other atmospheric constituents to produce HgII compounds (Shah

Previous work comparing GEOS-Chem model output against ambient measurements of Hg^{II} taken by a cation exchange membrane-based Hg^{II} measurement system concluded that although modeled total $Hg\ (Hg^0 + Hg^{II})$ concentrations matched well with observations, Hg^{II} was significantly lower in the model when compared to observations (Gratz et al., 2015; Shah et al., 2016). Later work included photoreduction of Hg^I and Hg^{II} to Hg^0 in the GLEMOS model which resulted in an overestimation of modeled Hg^0 and an underestimation of Hg^{II} , implying a missing oxidation pathway in the model (Saiz-Lopez et al., 2020).

An updated redox mechanism that includes photoreduction has been implemented in the GEOS-Chem model (Shah et al., 2021), but many aspects of the model are uncertain, including (but not limited to) atmospheric Br concentrations, rate coefficients for a number of the reactions in the chemical mechanism, gas-aerosol partitioning rates, and deposition processes. Shah et al. (2021) compared global annual average modeled HgII to KCl denuder-based HgII measurements, but because KCl denuder-based measurements are unreliable, the implications of these comparisons are unclear (see Fu et al., 2024 for a similar analysis with a different model platform). Gustin et al. (2023) compared direct cation exchange membrane samples collected over 1- or 2-week periods to GEOS-Chem with the Shah et al. (2021) chemistry and found that, while the model predicted HgII within the range of measurements at some locations, it drastically underestimated at other locations.

In this work, we compared GEOS-Chem results against Hg measurements at Storm Peak Laboratory in Colorado, USA, during a period with high Hg^{II} that has been shown to have originated from the free troposphere (Derry et al., 2024). These data were collected with a cation exchange membrane-based Hg measurement system that quantitatively

recovered Hg^{II} halide compounds introduced from a calibrator traceable to International System of Units (SI) standards (Elgiar et al., 2024). We used a series of sensitivity analyses to attempt to improve model-measurement agreement, and we analyzed the measurement and model datasets to gain insight as to the causes of the discrepancy.

This work was part of a larger study investigating atmospheric Hg behavior at Storm Peak Laboratory. Elgiar et al. (2024) detailed the Hg measurement system for the study and showed it can accurately quantify Hg⁰ and Hg^{II}. Derry et al. (2024) investigated the sources and behavior of Hg at Storm Peak over the entire measurement period (spring through fall 2021 and 2022). Lee et al. (2024) investigated the potential of iodine radical as a missing Hg⁰ oxidant. Weiss-Penzias et al. (2025) explored the effects of precipitation on Hg⁰ and Hg^{II} at Storm Peak and other locations.

2 Methods

2.1 Measurements of Hg

Ambient Hg^0 and Hg^{II} were measured using a dual channel measurement system developed by the Bingham Research Center at Utah State University. Details about the Hg measurement system were given by Elgiar et al. (2024). The dual channel system pulled air though a heated inlet (110 °C) with an elutriator and impactor designed to remove particles with an aerodynamic diameter greater than 2.5 µm at a total flow rate of 9L min⁻¹. Airflow from the inlet was routed sequentially through each of two channels to a Tekran 2537X Hg⁰ analyzer. One channel contained a thermal converter heated to 650 °C that converted all Hg in the sample to only Hg⁰, measuring total Hg. The other channel contained a series of two cation exchange membranes, which have been shown to quantitatively collect HgII while allowing Hg⁰ to pass through (Miller et al., 2019), measuring Hg⁰ only. HgII was calculated as the difference between the two channels. Hg⁰ and Hg^{II} measurements were calibrated while sampling ambient air with an automated, SI-traceable permeation tube-based calibrator, also developed at the Bingham Research Center. Permeation tubes containing HgBr₂ or Hg⁰ were housed in a temperature-controlled oven at 70 °C. Ultra-high purity nitrogen was used to carry the gas emitted from the tubes out of heated lines and into the inlet of the dual channel system. Flow was controlled by a critical orifice downstream of the permeation tubes, and a multiport valve was used to select between different tubes.

This measurement and calibration system had a 1 h detection limit for Hg^{II} of $6\text{--}12\,pg\,m^{-3}$ and recovered $97\pm4\,\%$ and $100\pm8\,\%$ (\pm standard deviation) of Hg^0 and $HgBr_2$, respectively. The expanded uncertainty (Elgiar et al., 2024; NIST, 2012) of Hg^0 and Hg^{II} were both 16 %. More details about instrument performance were given by Elgiar et al. (2024).

2.2 Sampling location and period

The dual channel system and automated calibrator were deployed at Storm Peak Laboratory (SPL) in Steamboat Springs Colorado, USA, from March 2021 to September 2022. Measurement-model comparisons in this study focused on an elevated Hg^{II} episode in June 2021 that was characterized by Derry et al. (2024). Storm Peak Laboratory is a permanent mountaintop atmospheric monitoring station located at 40.455° N, -106.744° W and 3220 m above sea level (Fig. 1). Previous Hg^{II} measurements at Storm Peak showed elevated concentrations measured by a system that utilized a KCl-coated denuder (Faïn et al., 2009). This is the first time that a cation exchange membrane-based system has been used to measure Hg^{II} at Storm Peak.

2.3 GEOS-Chem model

The GEOS-Chem 3D photochemical transport model (v12.8.0, DOI: https://doi.org/10.5281/zenodo.3784796, The International GEOS-Chem User Community, 2020), using Hg chemistry implemented by Shah et al. (2021), simulated Hg concentrations in the atmosphere. Simulations were performed for the period of 5 to 15 June 2021. Lee et al. (2024) conducted a comparison of measured and modeled ozone, temperature, and water vapor for the same base model used in this study.

A total of five separate simulations were carried out (Table 1), including two base model simulations and three separate sensitivity analyses using modified reaction rates (Table 2). The first base model simulation (Base 0.25×0.3125) used boundary conditions generated by a global simulation with horizontal resolution of $2^{\circ} \times 2.5^{\circ}$ to run a North American (10 to 60° latitude, -130 to -60° longitude) nested grid simulation at $0.25^{\circ} \times 0.3125^{\circ}$ resolution. The second base model simulation (Base 2×2.5) was a $2^{\circ} \times 2.5^{\circ}$ resolution global simulation with no nested simulation. Sensitivity analyses (SA1, SA2, and SA3) were conducted using $2^{\circ} \times 2.5^{\circ}$ global resolution, and comparisons were made only to the 2° × 2.5° resolution base model. Goddard Earth Observing System-Forward Processing (GEOS-FP) meteorology was used as input for all simulations. The only change to default Hg emissions used by Shah et al. was that Hg emissions from biomass burning events were updated to year 2021 using beta files produced by the Global Fire Emissions Database (Randerson et al., 2017). Daily oxidant files at $2^{\circ} \times 2.5^{\circ}$ resolution were produced from a full chemistry simulation using GEOS-Chem version 13.2.1 (The International GEOS-Chem User Community, 2022; information about different versions is available from the GEOS-Chem wiki (GEOS-Chem versions, 2025); see additional information about the full chemistry simulation in Lee et al., 2024). Each simulation was a reduced 47-layer simulation run with a spin-up time of 1 year. A spin-up time of 3 years was tested, and average modeled Hg⁰ and Hg^{II} concentrations at SPL during the sampling period increased by only 60 and 1 pg m⁻³, respectively. Thus, it was determined that a spin-up time of 1 year was sufficient for the purposes of this study.

The reactions of focus in the sensitivity analyses were: (1) the three-body reaction involving the oxidation of Hg^0 by Br (Reaction R1), (2) the three-body thermolysis reaction involving the dissociation of HgOH to produce Hg^0 and OH (Reaction R2), (3) the reaction of HgBr and O_3 to produce HgBrO and O_2 (Reaction R3) and (4) the reaction of HgOH and O_3 to produce HgOHO and O_2 (Reaction R4) (Table 2). We also conducted additional sensitivity tests of the SA1 scenario wherein the photoreduction frequency was increased iteratively to allow for Hg^0 closer to observed values, following Shah et al. (2021).

Experiments determining k for (Reaction R1) have ranged from $k = 1.46 \times 10^{-32} \text{ cm}^3 \text{ molec.}^{-1} \text{ s}^{-1}$ (Donohoue et al., 2006) to $k = 1.46 \times 10^{-31}$ cm³ molec. $^{-1}$ s⁻¹ (Ariya et al., 2002). We acknowledge that the Ariya et al. (2002) rate constant is unlikely to be representative of reality because of probable confounding effects from wall reactions (Donohoue et al., 2006). It is included in a sensitivity analysis here as a highest-case scenario. Rate coefficients for the reactions involving OH and Hg depend on calculations of the bond strength between OH and Hg, which has not yet been experimentally determined (Castro et al., 2022; Hewa Edirappulige et al., 2023). It was noted by Shah et al. (2021) that a minor change to this bond strength may have a substantial impact on Hg^{II} production in the model, which is important when considering k for Reaction (R2). Furthermore, Castro et al. (2022) recommended a $k = 7.5 \times 10^{-11}$ for Reactions (R3) and (R4), which is 2.4 times higher than the value for k used in the base model.

We performed sensitivity simulations with reduced dry and wet deposition rates using GEOS-Chem version 14.1 because the variables that drive deposition can be much more easily manipulated in this version. We used GEOS-FP meteorology and default Hg emissions and chemistry. Several updates and bug fixes related to Hg were implemented between versions 12.8 and 14.1 (GEOS-Chem versions, 2025). Hg⁰ in our version 14.1 base model averaged 87 % of concentrations in version 12.8, and HgII was 91 % of concentrations in version 12.8. To reduce Hg^{II} deposition in version 14.1, we manipulated variables for Hg_CHEM_PROP, which determines deposition for Hg^{II} species, in the species_database.yml file. We reduced dry deposition by changing the DD_ Hstar variable from 1.0×10^{14} to 1.0×10^{5} . We reduced wet deposition by changing the Henry_K0 variable from 1.40×10^6 to 1.40×10^4 .

2.4 Data processing and analysis

Daily average Hg concentrations were extracted from GEOS-Chem model output at the latitude and longitude of Storm Peak Laboratory and the corresponding vertical level in the model closest to Storm Peak Laboratory's elevation above



Figure 1. Location of Hg measurements at Storm Peak Laboratory, Colorado, USA.

Table 1. Descriptions of the different base model simulations and chemistry sensitivity analyses (SAs) using GEOS-Chem.

Simulation name	Description
Base 0.25 × 0.3125	$0.25^{\circ} \times 0.3125^{\circ}$ resolution base model run implementing the original k values used in Shah et al. (2021).
Base 2×2.5	$2^{\circ} \times 2.5^{\circ}$ resolution base model run implementing the original k values used in Shah et al. (2021).
SA1	Sensitivity analysis increasing k for Reaction (R1)
SA2	Sensitivity analysis decreasing k for Reaction (R2)
SA3	Sensitivity analysis increasing k for Reactions (R3) and (R4)

sea level (the model terrain height was lower than the actual elevation because of the model's coarse horizontal resolution). The sum of all Hg^I and Hg^{II} species in the model (gas and particle phases) was used for comparison with Hg^{II} measurements made by the dual-channel system. Only the Hg mass of oxidized Hg species was used, since only Hg mass is measured by the dual-channel analyzer. Model performance was evaluated using methods recommended by Chang and Hanna (2004). Processing of model outputs was performed with Python version 3.11, including with the GCPy toolkit. Statistical analyses were performed using Microsoft Excel, except that RMA regression was performed in Python with the pylr2 package. All data are reported as daily values \pm the 95 % confidence interval, unless otherwise specified.

3 Results and discussion

3.1 Observations of Hg

The time period of interest for this study, 7 to 11 June 2021, was an episode of elevated Hg^{II}. Hg^{II} reached a maximum of 212 pg m⁻³ on 9 June and was 23 % of the measured Hg⁰ at that time. An Hg^{II}/Hg⁰ ratio of 0.18 is considered high and indicative of in-situ oxidation (Timonen et al., 2013). Ten-day HYSPLIT backwards trajectories with GDAS input meteorology (Draxler and Rolph, 2010) for this day showed a mix of air originating high in the troposphere above the Pacific Ocean off the East Asian coast and lower in the troposphere near the Western coast of Mexico (Fig. 2). Aver-

Table 2. Summary of the rate coefficients (k) for the base model and modified k values for the sensitivity analyses. Units are cm³ molec.⁻¹ s⁻¹ for bimolecular reactions (Reactions R3 and R4) for cm⁶ molec.⁻² s⁻¹ for k_0 of three-body reactions (Reactions R1 and R2).

Reaction ID	Reaction	Base k	Modified k
(R1)	$\mathrm{Hg^0} + \mathrm{Br} + M \to \mathrm{BrHg^I} + M$	1.46×10^{-32}	1.46×10^{-31}
(R2)	$Hg^{I}OH + M \rightarrow Hg^{0} + O + H + M$	1.22×10^{-9}	1.22×10^{-10}
(R3)	$Hg^{I}Br + O_3 \rightarrow Hg^{II}BrO + O_2$	3×10^{-11}	7.5×10^{-11}
(R4)	$Hg^{I}OH + O_3 \rightarrow Hg^{II}OHO + O_2$	3×10^{-11}	7.5×10^{-11}

age observed $\mathrm{Hg^{II}}$ and $\mathrm{Hg^0}$ concentrations during the episode were $151\pm74\,\mathrm{pg\,m^{-3}}$ and $1.08\pm0.19\,\mathrm{ng\,m^{-3}}$, respectively. Observed $\mathrm{Hg^{II}}$ and $\mathrm{Hg^0}$ exhibited a strong anti-correlation ($r^2=0.91$), a phenomenon also observed by others who have measured Hg at SPL (Faïn et al., 2009). More details concerning this and other elevated $\mathrm{Hg^{II}}$ episodes at Storm Peak can be found in Derry et al. (2024).

3.2 Temporal trends and magnitude of Hg^{II} and Hg⁰

All simulations captured the observed temporal trends of $\mathrm{Hg^{II}}$ and $\mathrm{Hg^{0}}$, which indicates that GEOS-Chem accurately simulated the air mass transport event observed during the episode (Figs. 3 and 4; S2 and S3 in the Supplement show the same data on different scales to emphasize temporal trends in modeled data). Regression analysis comparing observed and modeled $\mathrm{Hg^{0}}$ and $\mathrm{Hg^{II}}$ showed moderate to strong correlations with measurements, ranging from $R^2 = 0.54$ to 0.79 (Figs.ur 5 and S1; Table 3). Despite these temporal correlations, none of the simulations was able to accurately capture the magnitude of the episode. Measured $\mathrm{Hg^{II}}$ reached a maximum of 19 % of total Hg compared with 14 % for SA1 and much lower values in the other simulations.

Table 3 and comprehensive statistical analyses in Table S1 in the Supplement show that simulated Hg⁰ was within the range of observations, except for SA1. Simulated Hg^{II}, however, was consistently much lower than observations. Simulations underpredicted average observed Hg^{II} by between 3.2 and 4.2 times.

The highest average modeled Hg^{II} occurred in SA1 and was $38\pm12\,pg\,m^{-3}$ (Table 3). A GEOS-Chem sensitivity analysis with the same change in the Hg+Br rate constant as SA1 was performed by Shah et al. (2016) and Gratz et al. (2015). They showed that increasing the rate constant led to an approximate two-fold increase in Hg^{II} , but the model continued to underestimate Hg^{II} measurements by up to three times. In this study, SA1 resulted in only a 30 % increase in Hg^{II} . Unlike the current study, Shah et al. (2016) increased rates of in-cloud reduction of Hg^{II} to Hg^0 to maintain the burden of total Hg in the simulated atmosphere. Hg^{II} likely did not increase as much in SA1 compared to Shah et al. (2016) because total Hg decreased substantially in SA1.

Overall, modifying kvalues in SA1, SA2, and SA3 did not have a large impact on HgII concentrations in the model, only increasing average Hg^{II} concentrations by 9, 8, and 5 pg m⁻³, respectively, when compared to the base model. The largest impact on modeled HgII was stratospheric HgII production in SA1, reaching a maximum of $\sim 900 \,\mathrm{pg}\,\mathrm{m}^{-3}$, compared to $\sim 600 \,\mathrm{pg}\,\mathrm{m}^{-3}$ in the base simulation, likely due to the abundance of Br in the stratosphere (Salawitch et al., 2005). Maximum stratospheric HgII values in SA2 and SA3 remained similar to the base simulation (Fig. 6). Others have shown evidence that the stratosphere is important to the overall atmospheric HgII load (Lyman and Jaffe, 2012; Murphy et al., 2006; Saiz-Lopez et al., 2025). Derry et al. (2024) did not find evidence that the air mass in this study originated in the stratosphere, though it is possible that a more generalized influence from the stratosphere did influence HgII concentra-

GEOS-Chem users typically adjust the photoreduction frequency of organic particulate Hg^{II} to match observed global Hg^0 ...(Shah et al., 2021; Horowitz et al., 2017). Since SA1 resulted in Hg^0 much lower than measurements, we conducted a set of sensitivity analyses that had the same modified Hg^0 + Br reaction rate as SA1, but wherein the photoreduction frequency was increased to allow for more Hg^0 , with a maximum increase of 2000 times above than the default value. Hg^0 increased in these sensitivity analyses, but Hg^{II} stayed within the same range (Figure S4). We hypothesize that the decrease in total Hg^{II} caused by the increase in photoreduction frequency was balanced by an increase in Hg^{II} because more Hg^0 was available for oxidation.

3.3 Relationship between Hg^{II} and Hg⁰

While all simulations resulted in a negative $Hg^{II}: Hg^0$ slope, simulated slopes were less negative than observations (Table 3; Fig. 7). An $Hg^{II}: Hg^0$ slope of -1 can be expected for a well-mixed air mass in which no addition or loss of Hg occurs (since Hg mass is conserved). Reduction of Hg^{II} back to Hg^0 or uptake of Hg^{II} by aerosols would maintain the -1 slope (assuming our instrument accurately measures aerosol-phase Hg). Assuming no addition or loss of Hg^0 , a slope greater than -1 (i.e., less negative) should indicate that a portion of Hg^{II} was lost from the air mass via dry or wet de-

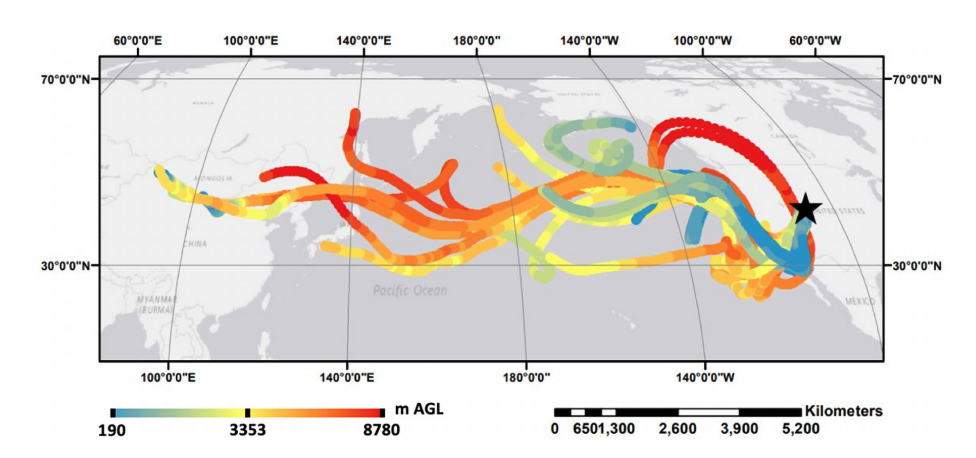


Figure 2. Ten-day HYSPLIT backwards trajectories ending on 9 June 2021. The black star represents the location of Storm Peak Laboratory.

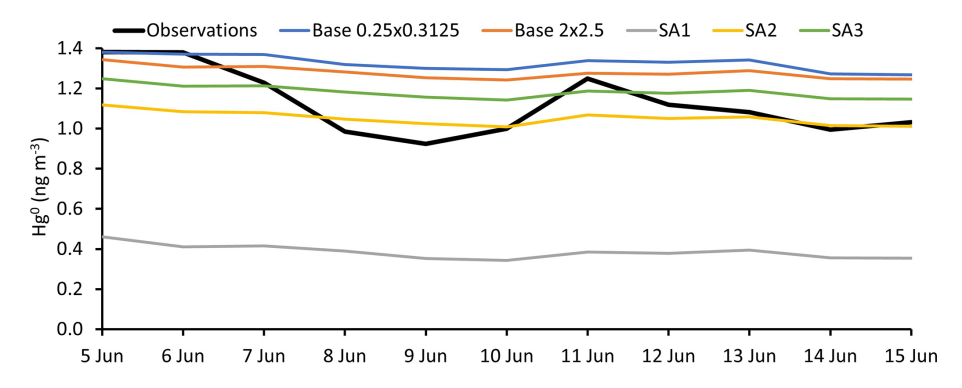


Figure 3. Observed and simulated daily average Hg⁰ from 5 to 15 June 2021.

position after it was produced (Swartzendruber et al., 2006; Lyman and Jaffe, 2012). Since all the simulations resulted in a greater Hg^{II} : Hg^{0} slope than the observations, we hypothesized that Hg^{II} depositional processes are overestimated in GEOS-Chem. To test this, we performed additional sensitivity tests with GEOS-Chem version 14.1 wherein Hg^{II} dry and wet deposition rates in GEOS-Chem were reduced, but we found an increase, rather than a decrease, in slope (from -0.28 to -0.18; see Fig. S5). Further sensitivity tests to probe this issue are warranted but are beyond the scope of the current study.

The sensitivity simulations did not result in any meaning-ful changes in the slope relative to the Base 2×2.5 simulation, which is expected because depositional processes were not changed. This was the case even for SA1, wherein the rate of the Hg+Br reaction was increased by 10 times. The Hg^{II}: Hg⁰ slope of the higher-resolution Base 0.2×0.3125 simulation was the most similar to observations. It is possible that cloud and precipitation processes were simulated more accurately in Base 0.25×0.3125 , leading to more realistic deposition rates. Since Hg^{II} and Hg⁰ values were extracted from simulations at the elevation of Storm Peak Laboratory rather than at the model surface level, interaction with the surface (and dry deposition) may have been less in the sim-

ulated versus observed air mass. Also, it is possible that the observed and simulated slopes greater than -1 were due to the confounding influence of a separate low-Hg 0 air mass that increasingly impacted the measurement location as Hg $^{\rm II}$ increased. This could be the case if the air mass was affected by the stratosphere, though Derry et al. (2024) did not find evidence for this.

While $\mathrm{Hg^{II}}:\mathrm{Hg^0}$ slopes close to -1 have been observed (Swartzendruber et al., 2006; Lyman and Jaffe, 2012), slopes greater than -1, as found in this study, have been more commonly found in other studies (Lyman and Jaffe, 2012; Fu et al., 2021). Derry et al. (2024) classified the period modeled in this work as two separate high $\mathrm{Hg^{II}}$ events: one from 7 through 11 June (their Event 4) and another from 13 through 15 June 2021 (their Event 5). They found $\mathrm{Hg^{II}}:\mathrm{Hg^0}$ slopes of -0.35 and -0.52, respectively, for the two periods. They identified a total of 18 high $\mathrm{Hg^{II}}$ events for the 2021–2022 measurement campaign with slopes ranging from -0.76 to -0.16, showing that $\mathrm{Hg^{II}}:\mathrm{Hg^0}$ slopes greater than -1 are common at Storm Peak Laboratory.

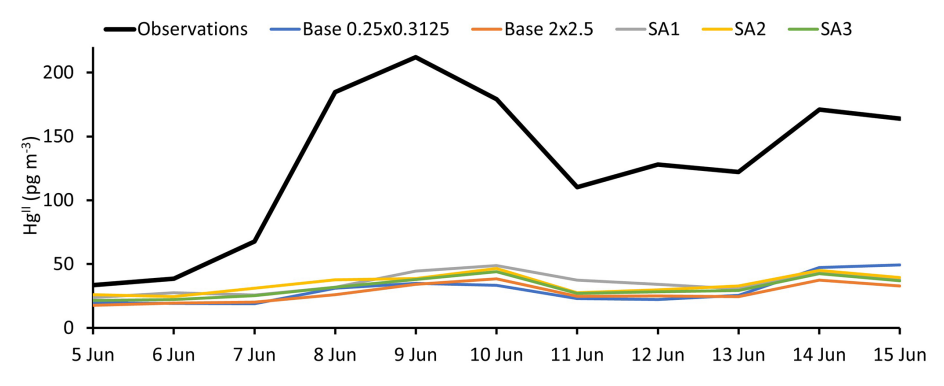


Figure 4. Observed and simulated daily average Hg^{II} from 5 to 15 June 2021.

Table 3. Summary of observed and modeled daily average Hg concentrations from 7 to 11 June 2021, and correlation between observed and simulated Hg. Averages are shown as average $\pm 95\%$ confidence interval. Slopes and intercepts were calculated using RMA regression. The ${\rm Hg^{II}:Hg^0}$ intercept is the ${\rm Hg^{II}}$ concentration at $0\,{\rm ng\,m^{-3}\,Hg^0}$.

	Avg. Hg^0 (ng m ⁻³)	Avg. Hg^{II} (pg m ⁻³)	Min. Hg ⁰ (ng m ⁻³)	Max. Hg ^{II} (pg m ⁻³)	Max. Hg ^{II} /Hg ⁰	Obs. vs. Sim. Hg^0 (r^2)	Obs. vs. Sim. Hg^{II} (r^2)	Hg ^{II} : Hg ⁰ slope	$Hg^{II}: Hg^0$ intercept $(pg m^{-3})$	$\begin{array}{c} \operatorname{Hg^{II}}:\operatorname{Hg^{0}} \\ (r^{2}) \end{array}$
Observations	1.08 ± 0.19	150 ± 74	0.92	212	0.23	_	_	-0.38	552	0.95
Base 0.25×0.3125	1.32 ± 0.04	28 ± 9	1.27	35	0.03	0.71	0.54	-0.28	397	0.89
Base 2×2.5	1.27 ± 0.03	29 ± 9	1.24	39	0.03	0.68	0.74	-0.23	323	0.86
SA1	0.38 ± 0.04	38 ± 12	0.34	49	0.14	0.69	0.67	-0.23	125	0.83
SA2	1.05 ± 0.04	36 ± 9	1.01	47	0.05	0.79	0.69	-0.22	261	0.79
SA3	1.18 ± 0.03	33 ± 10	1.14	44	0.04	0.73	0.75	-0.23	309	0.85

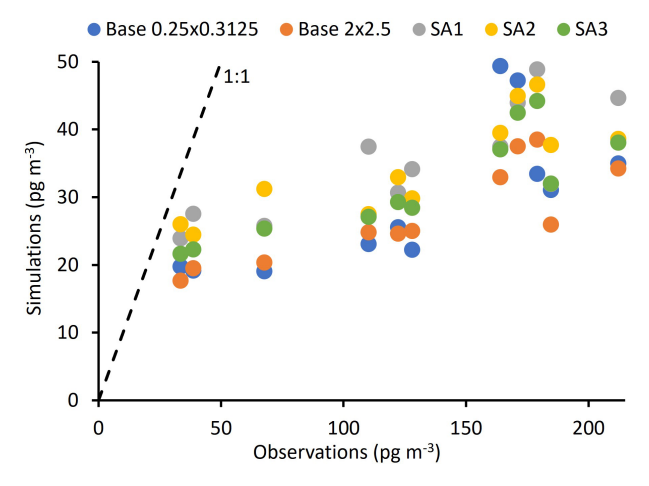


Figure 5. Observed versus simulated daily average Hg^{II} . A 1:1 slope is shown as a black dashed line.

3.4 Magnitude of changes in HgII and Hg0

The magnitude of the increase in Hg^{II} was calculated as the difference between the observed maximum Hg^{II} concentration during the high- Hg^{II} episode and the Hg^{II} concentration for 5 and 6 June, which were prior to the episode. The magnitude of the decrease in Hg^0 was calculated as the difference between the observed minimum Hg^0 concentration during the episode and the Hg^0 concentration for the days prior to

the episode. The observed change in magnitude for $\mathrm{Hg^{II}}$ and $\mathrm{Hg^0}$ was $176\,\mathrm{pg\,m^{-3}}$ and $-0.46\,\mathrm{ng\,m^{-3}}$, respectively. The modeled change in magnitude for $\mathrm{Hg^{II}}$ and $\mathrm{Hg^0}$, in contrast, ranged from 16 to $23\,\mathrm{pg\,m^{-3}}$ and -0.08 to -0.11, respectively.

Since Hg^{II} concentrations are influenced both by net oxidation and depositional loss, the change in magnitude of Hg⁰ is a better indicator to net oxidation during the episode (though we concede that Hg⁰ variability is also impacted by emissions, deposition, and transport phenomena, confounding the accuracy of this indicator). By this measure, observed net oxidation during the episode was about four times higher than simulations, including sensitivity simulations that increased oxidation reaction rates. Similarly, correlation between simulated and observed Hg⁰ is likely a more useful metric for model evaluation of redox processes than HgII correlations. By this measure, SA2 performed better than any of the other simulations, with an r^2 of 0.79. This better correlation could indicate that the reaction rate change employed in SA2 led to an oxidation environment that better matched reality.

3.5 Global Distribution of Hg

Maps showing global modeled Hg^{II} concentrations at the surface for Base 2 × 2.5, SA1, SA2, and SA3 are presented in Fig. 8. Surface Hg^{II} was higher in SA1, especially in the arc-

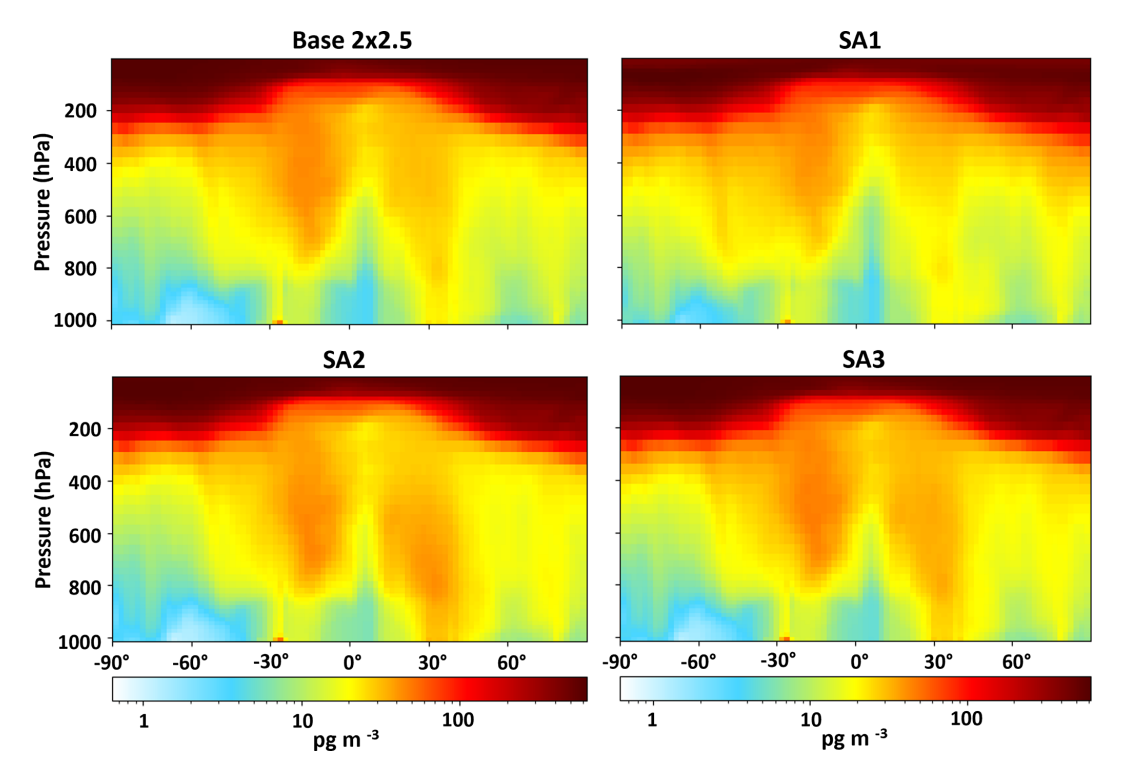


Figure 6. Global zonal mean plots for four of the GEOS-Chem simulations Hg^{II} on 9 June 2021.

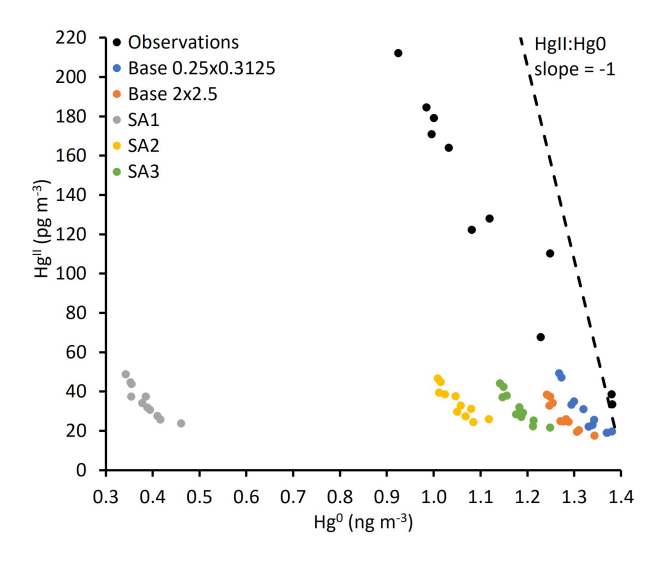


Figure 7. Relationship between daily average Hg^0 and Hg^{II} in observations and simulations. A -1:1 slope (shown as the black dashed line) indicates no addition or loss of Hg from the air mass. A slope greater than -1 (as shown in the measurement and model data) likely indicates depositional loss of Hg^{II} from the air mass.

tic and mid-latitude oceans. SA2 and SA3 showed only small increases in global Hg^{II} . Average modeled Hg^0 and total Hg concentrations for all simulations except SA1 were within 23 % or better of observations. SA1 showed a decrease in average Hg^0 of 65 % when compared to the base model. Shah

et al. (2016) did not show a decrease in Hg⁰ when performing a similar sensitivity analysis. This is because they increased rates of in-cloud reduction of Hg^{II} to Hg⁰ to maintain the burden of total Hg in the simulated atmosphere, which was not performed here. Figures 9 and S6 show increases to average dry and wet deposition for Hg^{II} in the base model and SA1 across the globe on 9 June 2021. This increased deposition likely explains the lower total Hg in the model. Further, natural and anthropogenic emissions of Hg are highly uncertain (Selin and Jacob, 2008; Zhu et al., 2016). It is also possible that emissions are too low in the model and that this is the cause of unrealistically low total Hg when Hg oxidation rates were adjusted in the sensitivity analyses.

3.6 Speciation of Hg^{II}

Of the 20 ${\rm Hg^{II}}$ species simulated at the measurement location (Fig. S7) in the Base 2×2.5 GEOS-Chem simulation, more than 99 % were comprised of aerosol-phase ${\rm Hg^{II}}$ (24 %) or gas-phase ${\rm HgCl_2}$ (72 %), ${\rm Hg(OH)_2}$ (3 %), and ${\rm HgBrOH}$ (1 %). Speciation was very similar in the sensitivity analyses. In SA1, for example, even though the rate of the ${\rm Hg+Br}$ reaction was increased by 10 times, ${\rm HgCl_2}$ still comprised 73 % of ${\rm Hg^{II}}$, with ${\rm HgBrOH}$, ${\rm HgOH_2}$, and aerosol ${\rm Hg^{II}}$ comprising 2 %, 1 %, and 24 %, respectively. In the model's chemical mechanism, any ${\rm Hg^{II}}$ sorbed to and subsequently volatilized from particles becomes ${\rm HgCl_2}$, which makes it the dominant ${\rm Hg^{II}}$ species in the model. Luippold et al. (2020) used an

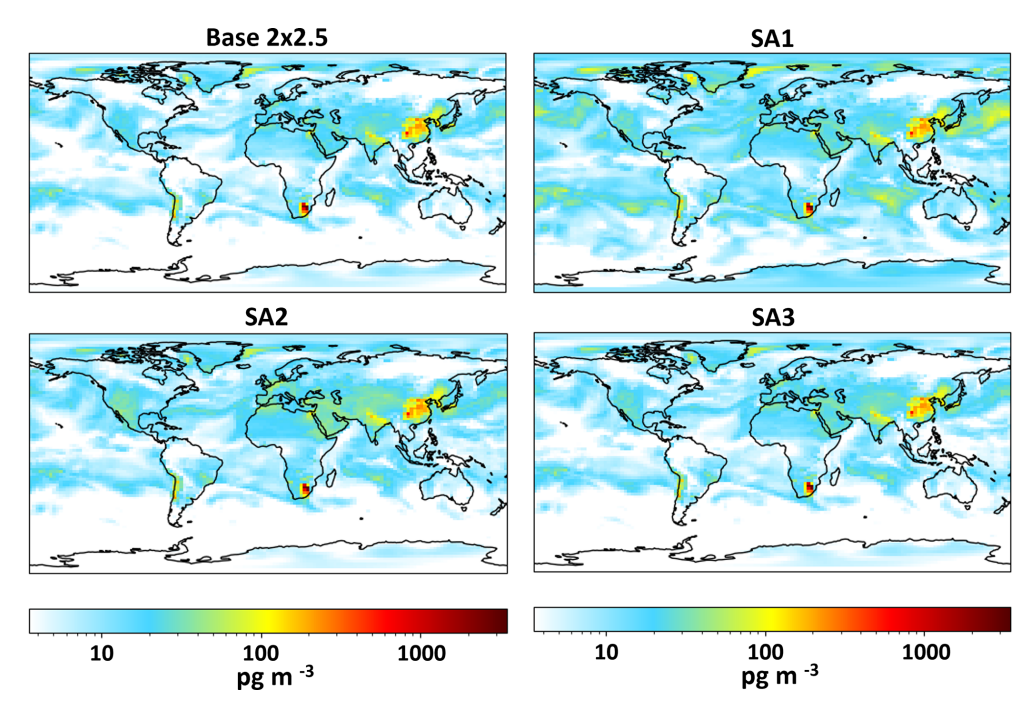


Figure 8. Average Hg^{II} concentrations at the surface on 9 June 2021 for four of the model simulations.

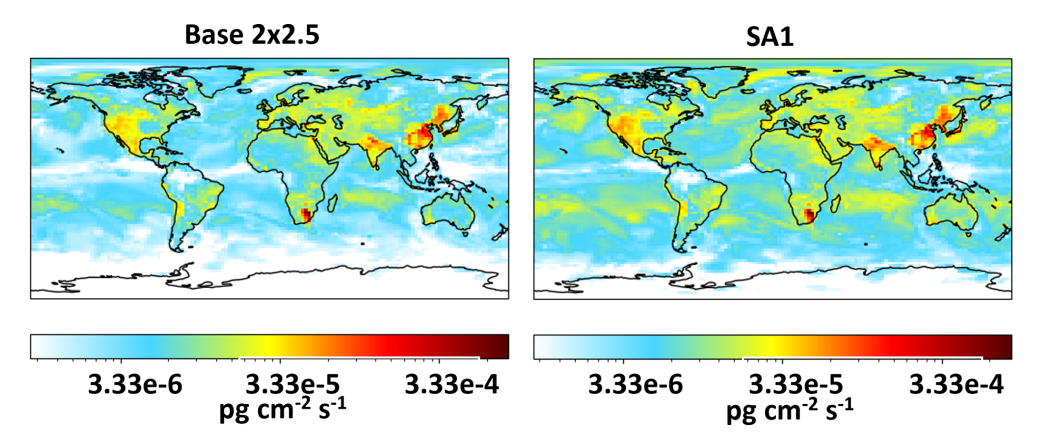


Figure 9. Average dry deposition for the Base 2×25 and SA1 simulations on 9 June 2021.

indirect thermal desorption method to show that nitrogenand sulfur-containing Hg compounds may make up a large fraction (up to 61 % and 69.7 %, respectively) of Hg^{II} compounds in ambient air, though primary oxidation of Hg⁰ by nitrogen- and sulfur-containing oxidants is not known to occur (Lyman et al., 2020b; Edirappulige et al., 2024). Nevertheless, one or more missing oxidation pathways could also help explain the underestimation of Hg^{II} in the model. Compound specific Hg^{II} measurement methods may help resolve this discrepancy (Khalizov et al., 2020; Lyman et al., 2020a).

3.7 Comparison with others' work

Shah et al. (2021) acknowledge a low Hg^{II} bias in their simulations of atmospheric Hg, especially in the free troposphere,

and note that (1) higher model Br does not solve the problem, and (2) modifications to aqueous Hg^{II} photoreduction and organic particulate Hg^{II} helps but requires unrealistic organic particulate Hg^{II} photoreduction rates. Similarly, our work shows a low Hg^{II} bias that is unresolvable with the current chemical mechanism. While Shah et al. (2021) focus on global mean conditions, however, the current work focuses on the dynamics of a specific high- Hg^{II} episode. We show that GEOS-Chem predicts Hg^{II} similar to measurements prior to the episode, and that the model simulates the timing and nature of the episode reasonably, but that the model's low bias for Hg^{II} appears to be driven by failure to adequately simulate the amount of Hg^{II} produced during the episode.

Table 4. Observed and modeled Hg^{II} from this study and from Gustin et al. (2023). All observations shown in the table, except those from this study, are from the RMAS direct Hg^{II} capture method. Model results from both studies used GEOS-Chem simulations with similar chemistry and other parameters. For this study, model output from the Base 2×25 simulation is shown. *P* values are from *t* tests.

	Observed Hg ^{II} (pg m ⁻³)	Modeled Hg ^{II} (pg m ⁻³)	Observed : modeled ratio	p value
Storm Peak Laboratory (low Hg ^{II} ; 5–7 June 2021)	47 ± 46	19 ± 3	2.4	0.12
Storm Peak Laboratory (high Hg ^{II} ; 8–15 June 2021)	159 ± 30	30 ± 5	5.2	< 0.01
Utah (October–December 2021)	12 ± 12	19 ± 5	0.6	0.13
Western Texas (October–December 2021)	93 ± 28	24 ± 5	3.8	< 0.01
Georgia (October–December 2021)	16 ± 4	9 ± 3	1.8	0.01
Indian Ocean (October–December 2021)	15 ± 6	8 ± 3	1.9	0.04
Nevada (June–July 2020)	133 ± 47	18 ± 4	7.4	< 0.01

Gustin et al. (2023) collected 1- or 2-week samples of Hg^{II} by direct capture on cation exchange membranes at locations in Nevada, Texas, Utah, and Georgia, USA, and at Reunion Island in the Indian Ocean. They used the same GEOS-Chem model setup as this study to compare GEOS-chem against their measurements. Table 4 shows the results of their comparison, along with a summary from this study. The simulation underpredicted the magnitude of HgII at all sites in the Gustin et al. study, except Utah, though model bias is relatively low for Georgia and the Indian Ocean. For Nevada and western Texas, observations were several times higher than model output, similar to the findings of this study. In some studies, high HgII has been measured in Utah (Lyman et al., 2022; Lan et al., 2012), and we expect that low Utah Hg^{II} in the Gustin et al. (2023) study was due to winter conditions at the site, though we acknowledge measurements in western Texas were also made during winter months. Simulated Hg^{II} at the Nevada location, which had the highest observed HgII in the Gustin et al. (2023) study, was in the same range as Utah, which had the lowest observed Hg^{II}.

In agreement with the current study, the Gustin et al. (2023) results show relatively low model bias at low-Hg^{II} locations and much higher bias at locations with high Hg^{II}. The relationship between measured Hg^{II} and the observed: modeled Hg^{II} ratio is linear and significant (p < 0.01; $r^2 = 0.82$; Fig. S8), showing that the GEOS-Chem low bias is predictable.

4 Conclusions

The purpose of this study was to investigate the ability of the GEOS-Chem 3D photochemical transport model to simulate a high-Hg^{II} episode observed at Storm Peak Laboratory in Colorado. The base GEOS-Chem reproduced

- 1. Hg⁰ concentrations to within 20 % of observations
- 2. Hg^{II} concentrations prior to the start of the high- Hg^{II} episode to within 50 %

3. The timing of changes in Hg^0 and Hg^{II} (R^2 of 0.54 to 0.79) which implies the model correctly simulated the transport of air masses that influenced the measurement site.

The model failed to reproduce:

- 1. The magnitude of temporal variability in Hg⁰ and Hg^{II} observed by the measurement system. Measured Hg^{II} and the measured decrease in Hg⁰ were both several times greater than simulations during the episode, including simulations with increased Hg⁰ oxidation rates. Under-simulation of the decrease in Hg⁰ is an indicator of underestimated net oxidation during the episode. Under-simulation of the increase in Hg^{II} is an indicator of underestimated net oxidation and/or overestimated Hg^{II} deposition.
- 1. The slope of the Hg^0 : Hg^{II} relationship during the episode. All simulations showed an inverse relationship, but the slope was more negative in the measurements than in the simulations. We infer from this that the model overestimated Hg^{II} deposition, though our measurements are inadequate to determine whether dry or wet deposition (or both) in the model led to the overestimate. Weiss-Penzias et al. (2025) investigated washout of Hg^{II} during precipitation events in the area of the study.

The results from Gustin et al. (2023) corroborated our findings, showing that the low bias of GEOS-Chem is worse when Hg^{II} is higher. Gratz et al. (2015) and Shah et al. (2016) both had similar findings, but they used a much simpler Hg chemical mechanism that only included oxidation of Hg⁰ by halogens. Our work provides evidence that the much more comprehensive Shah et al. (2021) still underrepresents Hg^{II} in some conditions, as acknowledged by Shah et al. (2021).

This study shows that the general causes of the model's low bias during high-Hg^{II} episodes are underestimation of net Hg⁰ oxidation and overestimation of Hg^{II} deposition. Some of this presumed bias could be due to intrusion of low-Hg⁰ stratospheric air into the studied air mass, but Derry et

al. (2024) found no evidence for stratospheric influence in this or other high-Hg^{II} air masses at Storm Peak Laboratory. Additional work is needed to elucidate the exact causes of the low bias.

Code and data availability. Measurement data collected during this project are publicly available at https://doi.org/10.5281/zenodo.10699270 (Gratz et al., 2024). GEOS-Chem model code is available at https://geoschem.github.io/index.html (last access: 3 August 2025).

Supplement. The supplement related to this article is available online at https://doi.org/10.5194/acp-25-16387-2025-supplement.

Author contributions. The primary contributor to the work is listed as the first author. The project lead is listed as the last author. Other authors are listed alphabetically. LEG, SNL, AGH, and RV planned the campaign. TRE, SNL, and LEG were responsible for Hg measurements. SNL and TRE developed and improved the dual-channel Hg measurement system. TRE and LD conducted GEOS-Chem modelling and analysis. TRE and SNL wrote the manuscript. TRE, SNL, LD, LEG, AGH, and RV reviewed and edited the manuscript.

Competing interests. At least one of the (co-)authors is a member of the editorial board of *Atmospheric Chemistry and Physics*. The peer-review process was guided by an independent editor, and the authors also have no other competing interests to declare.

Disclaimer. Publisher's note: Copernicus Publications remains neutral with regard to jurisdictional claims made in the text, published maps, institutional affiliations, or any other geographical representation in this paper. While Copernicus Publications makes every effort to include appropriate place names, the final responsibility lies with the authors. Views expressed in the text are those of the authors and do not necessarily reflect the views of the publisher.

Acknowledgements. The authors thank Ian McCubbin, Dan Gilchrist, and Maria Garcia for assisting with instrument maintenance and data acquisition. Trevor O'Neil helped design, build, and operate Hg instrumentation. Liji David provided GEOS-Chem model inputs and provided guidance and mentoring for the GEOS-Chem simulations.

Financial support. This research has been supported by the Directorate for Geosciences, Division of Atmospheric and Geospace Sciences (award nos. 1951513, 1951514, 1951515, and 1951632).

Review statement. This paper was edited by Aurélien Dommergue and reviewed by two anonymous referees.

References

- Ariya, P. A., Khalizov, A., and Gidas, A.: Reactions of gaseous mercury with atomic and molecular halogens: kinetics, product studies, and atmospheric implications, J. Phys. Chem. A, 106, 7310– 7320, 2002.
- Bu, X., Zhang, H., Lv, G., Lin, H., Chen, L., Yin, X., Shen, G., Yuan, W., Zhang, W., Wang, X., and Tong, Y.: Comparison of Reactive Gaseous Mercury Collection by Different Sampling Methods in a Laboratory Test and Field Monitoring, Environ. Sci. Tech. Let., 5, 600–607, https://doi.org/10.1021/acs.estlett.8b00439, 2018.
- Castro, P. J., Kellö, V., Cernušák, I., and Dibble, T. S.: Together, not separately, OH and O_3 oxidize $Hg^{(0)}$ to $Hg^{(II)}$ in the atmosphere, J. Phys. Chem. A, 126, 8266–8279, 2022.
- Chang, J. C. and Hanna, S. R.: Air quality model performance evaluation, Meteorol. Atmos. Phys., 87, 167–196, 2004.
- Derry, E. J., Elgiar, T. R., Wilmot, T. Y., Hoch, N. W., Hirshorn, N. S., Weiss-Penzias, P., Lee, C. F., Lin, J. C., Hallar, A. G., Volkamer, R., Lyman, S. N., and Gratz, L. E.: Elevated oxidized mercury in the free troposphere: analytical advances and application at a remote continental mountaintop site, Atmos. Chem. Phys., 24, 9615–9643, https://doi.org/10.5194/acp-24-9615-2024, 2024.
- Donohoue, D. L., Bauer, D., Cossairt, B., and Hynes, A. J.: Temperature and Pressure Dependent Rate Coefficients for the Reaction of Hg with Br and the Reaction of Br with Br: A Pulsed Laser Photolysis-Pulsed Laser Induced Fluorescence Study, J. Phys. Chem. A, 110, 6623–6632, 2006.
- Draxler, R. R. and Rolph, G. D.: HYSPLIT (HYbrid Single-Particle Lagrangian Integrated Trajectory) model, NOAA Air Resources Laboratory, Silver Spring, MD, https://www.ready.noaa.gov/HYSPLIT.php (last access: 8 October 2022), 2010.
- Dunham-Cheatham, S. M., Lyman, S., and Gustin, M. S.: Comparison and calibration of methods for ambient reactive mercury quantification, Sci. Total. Environ., 856, 159219, https://doi.org/10.1016/j.scitotenv.2022.159219, 2023.
- Edirappulige, D. H. T., Cheng, L., Castro, P., and Dibble, T.: Nitrate Radical Cannot Initiate Oxidation of Hg(0) to Hg(II) in the Laboratory or at Ground Level in the Atmosphere, ChemRxiv [preprint], https://doi.org/10.26434/chemrxiv-2024-qwh3w, 25 October 2024.
- Elgiar, T. R., Lyman, S. N., Andron, T. D., Gratz, L., Hallar, A. G., Horvat, M., Vijayakumaran Nair, S., O'Neil, T., Volkamer, R., and Živković, I.: Traceable Calibration of Atmospheric Oxidized Mercury Measurements, Environ. Sci. Technol., 58, 10706–10716, 2024.
- Faïn, X., Obrist, D., Hallar, A. G., Mccubbin, I., and Rahn, T.: High levels of reactive gaseous mercury observed at a high elevation research laboratory in the Rocky Mountains, Atmos. Chem. Phys., 9, 8049–8060, https://doi.org/10.5194/acp-9-8049-2009, 2009.
- Fu, X., Jiskra, M., Yang, X., Marusczak, N., Enrico, M., Chmeleff, J., Heimburger-Boavida, L.-E., Gheusi, F., and Sonke, J. E.: Mass-independent fractionation of even and odd mercury isotopes during atmospheric mercury redox reactions, Environ. Sci. Technol., 55, 10164–10174, 2021.
- Fu, X., Sun, X., Travnikov, O., Li, Q., Qin, C., Cuevas, C. A., Fernandez, R. P., Mahajan, A. S., Wang, S., Wang, T., and Saiz-Lopez, A.: Anthropogenic short-lived halogens increase hu-

- man exposure to mercury contamination due to enhanced mercury oxidation over continents, P. Natl. Acad. Sci. USA, 121, e2315058121, https://doi.org/10.1073/pnas.231505812, 2024.
- GEOS-Chem versions: (https://wiki.seas.harvard.edu/geos-chem/index.php/GEOS-Chem_versions, last access: 8 September 2025), 2025.
- Gratz, L., Ambrose, J., Jaffe, D., Shah, V., Jaeglé, L., Stutz, J., Festa, J., Spolaor, M., Tsai, C., Selin, N., Song, S., Zhou, X., Weinheimer, A., Knapp, D. J., Montzka, D. D., Flocke, F., Campos, T., Apel, E. C., Hornbrook, R. S., Blake, N., Hall, S., Tyndall, G., Reeves, M., Stechman, D., and Stell, M.: Oxidation of mercury by bromine in the subtropical Pacific free troposphere, Geophys. Res. Lett., 42, 10494–10502, 2015.
- Gratz, L., Lyman, S., Elgiar, T., Hallar, A. G., and Volkamer, R.: Measurements of atmospheric mercury, trace gases, aerosols, and meteorology at Storm Peak Laboratory, Colorado, in 2021 and 2022, Version 1, Zenodo [data set], https://doi.org/10.5281/zenodo.10699270, 2024.
- Gustin, M. S., Dunham-Cheatham, S. M., Allen, N., Choma, N., Johnson, W., Lopez, S., Russell, A., Mei, E., Magand, O., Dommergue, A., and Elgiar, T.: Observations of the chemistry and concentrations of reactive Hg at locations with different ambient air chemistry, Sci. Total. Environ., 904, 166184, https://doi.org/10.1016/j.scitotenv.2023.166184, 2023.
- Hewa Edirappulige, D. T., Kirby, I. J., Beckett, C. K., and Dibble, T. S.: Atmospheric Chemistry of HOHg^(II)O* Mimics That of a Hydroxyl Radical, J. Phys. Chem. A, 127, 8392–8403, 2023.
- Horowitz, H. M., Jacob, D. J., Zhang, Y., Dibble, T. S., Slemr, F., Amos, H. M., Schmidt, J. A., Corbitt, E. S., Marais, E. A., and Sunderland, E. M.: A new mechanism for atmospheric mercury redox chemistry: implications for the global mercury budget, Atmos. Chem. Phys., 17, 6353–6371, https://doi.org/10.5194/acp-17-6353-2017, 2017.
- Huang, J. and Gustin, M. S.: Uncertainties of Gaseous Oxidized Mercury Measurements Using KCl-Coated Denuders, Cation-Exchange Membranes, and Nylon Membranes: Humidity Influences, Environ. Sci. Technol., 49, 6102–6108, 2015.
- Jiao, Y. and Dibble, T. S.: First kinetic study of the atmospherically important reactions BrHg*+ NO₂ and BrHg*+ HOO, Phys. Chem. Chem. Phys., 19, 1826–1838, 2017a.
- Jiao, Y. and Dibble, T. S.: Structures, Vibrational Frequencies, and Bond Energies of the BrHgOX and BrHgXO Species Formed in Atmospheric Mercury Depletion Events, J. Phys. Chem. A, 121, 797-7985, 2017b.
- Khalizov, A. F., Guzman, F. J., Cooper, M., Mao, N., Antley, J., and Bozzelli, J.: Direct detection of gasphase mercuric chloride by ion drift-Chemical ionization mass spectrometry, Atmos. Environ., 238, 117687, https://doi.org/10.1016/j.atmosenv.2020.117687, 2020.
- Lam, K. T., Wilhelmsen, C. J., Schwid, A. C., Jiao, Y., and Dibble, T. S.: Computational Study on the Photolysis of BrHgONO and the Reactions of BrHgO with CH₄, C₂H₆, NO, and NO₂: Implications for Formation of Hg(II) Compounds in the Atmosphere, J. Phys. Chem. A, 123, 1637–1647, 2019.
- Lan, X., Talbot, R., Castro, M., Perry, K., and Luke, W.: Seasonal and diurnal variations of atmospheric mercury across the US determined from AMNet monitoring data, Atmos. Chem. Phys., 12, 10569–10582, https://doi.org/10.5194/acp-12-10569-2012, 2012.

- Lee, C. F., Eligar, T., David, L. M., Wilmot, T. Y., Reza, M., Hirshorn, N., McCubbin, I. B., Shah, V., Lin, J. C., Lyman, S. N., Hallar, A. G., Gratz, L. E., and Volkamer, R.: Elevated Tropospheric Iodine over the Central Continental United States: Is Iodine a Major Oxidant of Atmospheric Mercury?, Geophys. Res. Lett., 51, e2024GL109247, https://doi.org/10.1029/2024GL109247, 2024.
- Luippold, A., Gustin, M. S., Dunham-Cheatham, S. M., and Zhang, L.: Improvement of quantification and identification of atmospheric reactive mercury, Atmos. Environ., 224, 117307, https://doi.org/10.1016/j.atmosenv.2020.117307, 2020.
- Lyman, S. N. and Jaffe, D. A.: Elemental and oxidized mercury in the upper troposphere and lower stratosphere, Nat. Geosci., 5, 114–117, 2012.
- Lyman, S. N., Jaffe, D. A., and Gustin, M. S.: Release of mercury halides from KCl denuders in the presence of ozone, Atmos. Chem. Phys., 10, 8197–8204, https://doi.org/10.5194/acp-10-8197-2010, 2010.
- Lyman, S. N., Cheng, I., Gratz, L. E., Weiss-Penzias, P., and Zhang, L.: An updated review of atmospheric mercury, Sci. Total. Environ., 707, 135575, https://doi.org/10.1016/j.scitotenv.2019.135575, 2020a.
- Lyman, S. N., Gratz, L. E., Dunham-Cheatham, S. M., Gustin, M. S., and Luippold, A.: Improvements to the accuracy of atmospheric oxidized mercury measurements, Environ. Sci. Technol., 54, 13379–13388, 2020b.
- Lyman, S. N., Elgiar, T., Gustin, M. S., Dunham-Cheatham, S. M., David, L. M., and Zhang, L.: Evidence against Rapid Mercury Oxidation in Photochemical Smog, Environ. Sci. Technol., 56, 11225–11235, 2022.
- Mahbub, K. R., Krishnan, K., Naidu, R., Andrews, S., and Megharaj, M.: Mercury toxicity to terrestrial biota, Ecol. Indic., 74, 451–462, 2017.
- McClure, C. D., Jaffe, D. A., and Edgerton, E. S.: Evaluation of the KCl denuder method for gaseous oxidized mercury using HgBr₂ at an in-service AMNet site, Environ. Sci. Technol., 48, 11437–11444, 2014.
- Miller, M. B., Dunham-Cheatham, S. M., Gustin, M. S., and Edwards, G. C.: Evaluation of cation exchange membrane performance under exposure to high Hg⁰ and HgBr₂ concentrations, Atmos. Meas. Tech., 12, 1207–1217, https://doi.org/10.5194/amt-12-1207-2019, 2019.
- Murphy, D. M., Hudson, P. K., Thomson, D. S., Sheridan, P. J., and Wilson, J. C.: Observations of mercury-containing aerosols, Environ. Sci. Technol., 40, 3163–3167, 2006.
- NIST: NIST/SEMATCH e-Handbook of Statistical Methods, https://doi.org/10.18434/M32189, 2012.
- Peng, X., Wang, W., Xia, M., Chen, H., Ravishankara, A. R., Li, Q., Saiz-Lopez, A., Liu, P., Zhang, F., Zhang, C., Xue, L., Wang, X., George, C., Wang, J., Mu, Y., Chen, J., and Wang, T.: An unexpected large continental source of reactive bromine and chlorine with significant impact on wintertime air quality, Natl. Sci. Rev., 8, nwaa304, https://doi.org/10.1093/nsr/nwaa304, 2021.
- Randerson, J., Van Der Werf, G., Giglio, L., Collatz, G., and Kasibhatla, P.: Global fire emissions database, Version 4.1 (GFEDv4), ORNL Distributed Active Archive Center [data set], https://doi.org/10.3334/ORNLDAAC/1293, 2017.
- Rice, K. M., Walker Jr, E. M., Wu, M., Gillette, C., and Blough, E. R.: Environmental mercury and its toxic effects,

- Journal of preventive medicine and public health, 47, 74–83, https://doi.org/10.3961/jpmph.2014.47.2.74, 2014.
- Saiz-Lopez, A., AcunPa, A. U., Trabelsi, T., Carmona-García, J., Daivalos, J. Z., Rivero, D., Cuevas, C. A., Kinnison, D. E., Sitkiewicz, S. P., Roca-Sanjuain, D., and Francisco, J.: Gas-Phase Photolysis of Hg (I) Radical Species: A New Atmospheric Mercury Reduction Process, J. Am. Chem. Soc., 141, 8698– 8702, 2019.
- Saiz-Lopez, A., Travnikov, O., Sonke, J. E., Thackray, C. P., Jacob, D. J., Carmona-García, J., Francés-Monerris, A., Roca-Sanjuán, D., Acuña, A. U., Dávalos, J. Z., Cuevas, C. A., Jiskra, M., WAng, F., Bieser, J., Plane, J. M. C., and Francisco, J. S.: Photochemistry of oxidized Hg (I) and Hg (II) species suggests missing mercury oxidation in the troposphere, P. Natl. Acad. Sci. USA, 117, 30949–30956, 2020.
- Saiz-Lopez, A., Cuevas, C. A., Acuña, A. U., Añel, J. A., Mahajan, A. S., de la Torre, L., Feng, W., Dávalos, J. Z., Roca-Sanjuán, D., and Kinnison, D. E.: Role of the stratosphere in the global mercury cycle, Science Advances, 11, eads1459, https://doi.org/10.1126/sciadv.ads1459, 2025.
- Salawitch, R. J., Weisenstein, D. K., Kovalenko, L. J., Sioris, C. E., Wennberg, P. O., Chance, K., Ko, M. K., and McLinden, C. A.: Sensitivity of ozone to bromine in the lower stratosphere, Geophys. Res. Lett., 32, L05811, https://doi.org/10.1029/2004GL021504, 2005.
- Selin, N. E. and Jacob, D. J.: Seasonal and spatial patterns of mercury wet deposition in the United States: Constraints on the contribution from North American anthropogenic sources, Atmos. Environ., 42, 5193–5204, 2008.
- Shah, V., Jacob, D. J., Thackray, C. P., Wang, X., Sunderland, E. M., Dibble, T. S., Saiz-Lopez, A., Černušák, I., Kellö, V., Castro, P. J., Wu, R., and Wang, C.: Improved mechanistic model of the atmospheric redox chemistry of mercury, Environ. Sci. Technol., 55, 14445–14456, 2021.
- Shah, V., Jaeglé, L., Gratz, L. E., Ambrose, J. L., Jaffe, D. A., Selin, N. E., Song, S., Campos, T. L., Flocke, F. M., Reeves, M., Stechman, D., Stell, M., Festa, J., Stutz, J., Weinheimer, A. J., Knapp, D. J., Montzka, D. D., Tyndall, G. S., Apel, E. C., Hornbrook, R. S., Hills, A. J., Riemer, D. D., Blake, N. J., Cantrell, C. A., and Mauldin III, R. L.: Origin of oxidized mercury in the summertime free troposphere over the southeastern US, Atmos. Chem. Phys., 16, 1511–1530, https://doi.org/10.5194/acp-16-1511-2016, 2016.

- Streets, D. G., Horowitz, H. M., Lu, Z., Levin, L., Thackray, C. P., and Sunderland, E. M.: Global and regional trends in mercury emissions and concentrations, 2010–2015, Atmos. Environ., 417–427, https://doi.org/10.1016/j.atmosenv.2018.12.031, 2019.
- Swartzendruber, P. C., Jaffe, D. A., Prestbo, E. M., Weiss-Penzias, P., Selin, N. E., Park, R., Jacob, D. J., Strode, S., and Jaeglé, L.: Observations of reactive gaseous mercury in the free troposphere at the Mt. Bachelor Observatory, J. Geophys. Res.-Atmos., 111, D24301, https://doi.org/10.1029/2006JD007415, 2006.
- Tang, Y., Wang, S., Li, G., Han, D., Liu, K., Li, Z., and Wu, Q.: Elevated gaseous oxidized mercury revealed by a newly developed speciated atmospheric mercury monitoring system, Environ. Sci. Technol., 56, 7707–7715, 2022.
- The International GEOS-Chem User Community: geoschem/geoschem: GEOS-Chem 12.8.0, Version 12.8.0, Zenodo [code], https://doi.org/10.5281/zenodo.3784796, 2020.
- The International GEOS-Chem User Community: geoschem/geoschem: GEOS-Chem 12.8.0, Version 13.2.1, Zenodo [code], https://doi.org/10.5281/zenodo.5500717, 2022.
- Timonen, H., Ambrose, J. L., and Jaffe, D. A.: Oxidation of elemental Hg in anthropogenic and marine airmasses, Atmos. Chem. Phys., 13, 2827–2836, https://doi.org/10.5194/acp-13-2827-2013, 2013.
- Weiss-Penzias, P. S., Lyman, S. N., Elgiar, T., Gratz, L. E., Luke, W. T., Quevedo, G., Choma, N., and Gustin, M. S.: The effect of precipitation on gaseous oxidized and elemental mercury concentrations as quantified by two types of atmospheric mercury measurement systems, Environmental Science: Atmospheres, 5, 204–219, https://doi.org/10.1039/D4EA00145A, 2025.
- Zhou, J. and Obrist, D.: Global mercury assimilation by vegetation, Environ. Sci. Technol., 55, 14245–14257, 2021.
- Zhu, W., Lin, C.-J., Wang, X., Sommar, J., Fu, X., and Feng, X.: Global observations and modeling of atmosphere–surface exchange of elemental mercury: a critical review, Atmos. Chem. Phys., 16, 4451–4480, https://doi.org/10.5194/acp-16-4451-2016, 2016.